DOI: 10.1021/ma900719a

Macromolecules
ARTICLE

Clipped Random Wave Morphologies and the Analysis of the SAXS of an Ionomer Formed by Copolymerization of Tetrafluoroethylene and CF_2=$CFO(CF_2)_4SO_3H$

Niccolo V. Aieta,[†] Ronald J. Stanis,[†] James L. Horan,[†] Michael A. Yandrasits,[‡] David J. Cookson,[§] Bridget Ingham,[⊥] Michael F. Toney,[||] Steven J. Hamrock,[‡] and Andrew M. Herring*,[†]

[†]*Department of Chemical Engineering, Colorado School of Mines, Golden, Colorado 80401,* [‡]*3M Fuel Cell Components Program, 3M Center, St. Paul, Minnesota 55144,* [§]*Australian Synchrotron, Clayton, VIC 3168, Australia,* [||]*Stanford Synchrotron Radiation Lightsource, Stanford Linear Accelerator Center, Menlo Park, California 94025, and* [⊥]*Industrial Research Limited, Lower Hutt, New Zealand*

Received April 3, 2009; Revised Manuscript Received June 24, 2009

ABSTRACT: Using SAXS data, the microstructure of the ionomer formed by copolymerization of tetrafluoroethylene and CF_2=$CFO(CF_2)_4SO_3H$ films has been approached by two methods: a numerical method (the unified fit approach) utilizing a simple model of spherical scattering objects to determine the radius of gyration of different scattering features of the ionomer films and by a graphical method, the clipped random wave approach (CRW), using the scattering data and a porosity parameter to generate a random wave which is clipped to produce a real-space image of the microstructure. We studied films with EW of 733, 825, 900, and 1082 in both the as-cast and annealed "dry" and boiled "wet" states. The results of the two data analysis techniques are in good size agreement with each other. In addition, the CRW model show striking similarities to the structure proposed in a recent dissipative particle dynamic models. This has been the first time to our knowledge that the CRW technique has been applied to a PFSA type ionomer.

1. Introduction

With the current interest in the more efficient use of primary energy sources, there is much interest in the use of fuel cells for energy conversion. These devices can operate at higher efficiencies than heat engines and also with zero pollution at the point of use and no net CO_2 emission when run on renewably produced hydrogen.[1] Of all the fuel cells being considered for commercial production, the proton exchange membrane (PEM) fuel cell has many advantages, including very high volumetric power density, facile load following, and relatively low temperature of operation allowing the device to be built from easy to process components. Two primary barriers to the commercial production of these devices are the unacceptably high loading of expensive Pt or Pt alloys in the cathode to facilitate the oxygen reduction reaction and the need for the PEM, typically a perfluorosulfonic acid (PFSA) ionomer, to be hydrated at 100% RH to achieve practical levels of proton conduction. The consequences of this second problem are that the fuel cell cannot be operated above 80 °C without impractical pressurization. In addition, water production at the cathode in the saturated air stream leads to flooding and water management issues, and RH cycling, e.g., between on and off conditions, leads to unacceptable mechanical membrane degradation.[2] In order to understand the effect of hydration on the mechanical strength and proton conductivity of PFSA PEMs, it is necessary to be able to understand the morphology of the polymers at a range of hydration states. If the microstructure can be known, it should be possible to molecularly engineer new more mechanically robust electrolytes with improved proton transport under drier and hotter operating conditions.

PFSA PEMs consist of a hydrophobic backbone consisting of repeating tetrafluoroethylene units with a hydrophilic sulfonated side chain. Available PFSA PEMs range from the well-known DuPont polymer Nafion with the a long sulfonic acid side chain, through a medium side chain polymer recently introduced by 3M, to the short side chain polymer originally synthesized by Dow but now marketed by Solvay-Solexis as Hyflon (Scheme 1).[3−5]

The state of understanding of Nafion has recently been reviewed.[5] The sulfonic acid content of a PFSA is usually reported as equivalent weight (EW), which is the number of grams of polymer to provide 1 mol equiv of acid. Lower EW ionomer membranes allow for increased proton conductivity due to the number of available protonic sites per volume.

The first model to find widespread acceptance for the morphology of water-swollen Nafion was best described by a model of ionic clusters that were approximately spherical in shape with an inverted micellar structure.[6] A more complete model of PFSA PEMs based on extensive X-ray and neutron scattering describes a hydrophobic framework of low-dimensional objects defining the boundary with the hydrophilic domain. In Nafion, the latter is well-connected, even at low degrees of hydration; i.e., there are almost no dead-end pockets, and the material exhibits very good percolation. Because of the side-chain architecture of Nafion, a third transition region describing the interaction between the aqueous domain and the hydrophobic polymer backbone has been introduced.[7,8] Dissipative particle dynamics (DPD) simulations of Nafion, the 3M ionomer, and the short side-chain ionomer now marketed as Hyflon have been performed by dividing each hydrated ionomer into components consisting of a common polytetrafluoroethylene backbone bead, ionomer specific backbone beads, a terminal side chain bead, and a bead consisting of a cluster of water molecules.[9−11] These simulations show that there is a bicontinuous phase of hydrophobic and hydrophilic regions with a continuous path of water in any direction. The calculations show that the clusters are irregular and in the case of Nafion show an uncanny resemblance to the

*Corresponding author. E-mail: aherring@mines.edu.

 Published on Web 07/14/2009

Scheme 1. Structures of PFSA PEMs (From Left to Right: Nafion, the 3M Ionomer, and Hyflon)

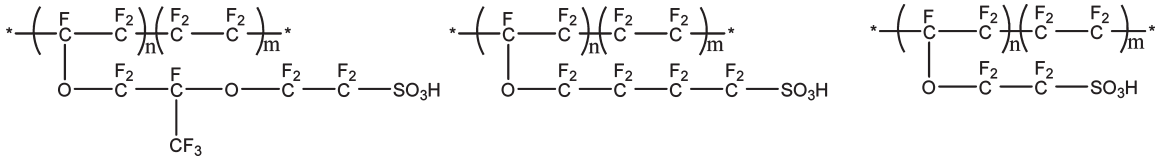

Fourier transformed SAXS data obtained by the maximum entropy method.[12]

In this work we analyze for the first time the SAXS patterns for various EW of the 3M ionomer both in their as-cast "dry" form and in their fully hydrated form after being boiled in water. We also show that the Fourier transformed 3D microstructures of these film have similarities with the DPD simulations of this PFSA PEM.

2. Experimental Section

2.1. Materials. The 3M ionomer was provided by the 3M Corp. in the form of a dispersion suitable for casting in the following equivalent weights: 733, 825, 900, and 1082. The 900 EW material was blended from 1000 and 836 EW polymers. All membranes were prepared by solution-casting from a polymer dispersion that was ~20 wt % solids. The remainder of the dispersion was a mixture of *n*-propanol and water (70%/30% by weight). The solutions were spread to a uniform thickness of 635 μm on Kapton film using a doctor blade. Solvent evaporation was performed at 80 °C followed by subsequent thermal annealing at 160 °C.

2.2. SAXS Measurements. SAXS Experiments were carried out at CHEMmat CARS, beamline 15, at the Advanced Photon Source (APS) located at the Argonne National Laboratory, Argonne, IL. All measurements were taken in transmission geometry and collected with a Bruker 6000 CCD detector (94 mm × 94 mm, 92 μm pixel size) using an acquisition time of 2 s. The 2D scatter was radially integrated providing plots of intensity versus the scattering vector q. The transmission intensity was normalized to exposure time and flux of the direct beam through the sample. However, because of the swelling of the samples tested, absolute thickness and atomic density could not be determined in situ. Therefore, the intensity units become arbitrary. The incoming X-ray wavelength (λ) was 1 ± 0.05 Å for all samples. The incident photon energy was known to 0.1 eV for each sample. Scattering was collected in a q range of 0.01−0.21 Å^{-1}.

Direct preparation of the ambient (dry) films consisted of removing the samples from the Kapton backing, cutting them to ~1 cm × 3 cm, and placing them in a sample holder for exposure. Hydrated (wet) measurements were made by placing samples in a beaker of boiling water for 1 h. Samples were removed from the boiling water, patted dry, and placed in the sample holder for SAXS measurements. Total time from boiling to the completion of the SAXS measurements was ~3 min.

3. SAXS Data Analysis

The data were fit using two complementary models: the unified fit approach was used as a quantitative tool to extract information about the size of the scattering features, and the clipped random wave morphology (CRW) method was used to generate a graphical representation of the morphology.

3.1. Numerical Fitting. The numerical fitting relates the scattering intensity, $I(q)$, to a summation of Gaussian functions. These are well understood "Guinier-type" functions.[13] Along with correlated interference interactions, this allows for simple modeling of the radius of gyration (R_g), packing density, and packing distances of the scattering objects in question.[14]

$$I(q) = \sum_{m=1}^{n} G_m e^{-q^2 R_g^2/3} \quad (1)$$

G is the Guinier prefactor and is linearly related to the number of particles that are contributing to the scatter by

$$G = n^2 N_p I_e \quad (2)$$

n is the number of electrons in a particle, N_p is the number of particles in contact with the incident beam, and I_e is the scattering factor for a single electron. The data for each sample were fitted using two Guinier functions. If necessary, a third power law function level was used in the summation to accurately represent the low q features. The power law function is

$$B_m\left(\frac{1}{q^p}\right) \quad (3)$$

where

$$B = 2\pi N_p \rho_e{}^2 S_p I_e \quad (4)$$

N_p is the number of particles in contact with the incident beam, ρ_e is the particle's electron density, S_p is the surface area of the particle, and I_e is the scattering factor for a single electron. Equation 3, when used, was truncated at a q value proportionate to the R_g of the lower level so as to not interfere with those fitting parameters.[15]

Correlations between particles in a given structural level are accounted for by calculating the constructive interference between two (or more) particles. Using the Born−Green approximation,[13,16] interactions between scattering objects are accounted for under the assumption that interferences can be described by a spherically symmetric correlation about the center of mass of a particle. The total scattering intensity for a structural level containing interacting particles is modified by the function

$$I(q)_{total} = I(q)\left(\frac{1}{(1+P_a) \times \text{sphere amplitude}(q,\eta)}\right) \quad (5)$$

where

$$\text{sphere amplitude}(q,\eta) = 3\left(\frac{\sin(q\eta) - q\eta\cos(q\eta)}{(q\eta)^3}\right) \quad (6)$$

Interferences are described by two parameters, P_a and η, where P_a is the packing factor, described by eq 7:

$$P_a = \frac{8\nu_H}{\nu_0} \quad (7)$$

ν_H is the hard-sphere volume, and ν_0 is the total occupied volume. P_a can have a value from 0 (no correlations) to ~5.82 (calculated for FCC or HCP packing) and should not be confused with the Porod exponent (P) in eq 3. η is the distance between the centers of the scattering objects in question. The value of η should be no less than the diameter of the particles and increases as the system becomes more

dilute. Using the Irena macros package[15] for the Igor Pro software (Wavemetrics Inc.), interparticle interactions within a given structural level were accounted for. No interactions between levels were possible with these tools.

3.2. CRW Technique. The second method employed to interpret the scattering data is a clipped random wave (CRW) technique. This technique is used to get a visual representation of the polymer film on the nanoscale. CRW methods are a model-independent approach, which will produce the most likely structure consistent with experimental scattering data, with very limited a priori assumptions. The CRW technique is used to visualize the real-space morphology of the ionomer by transforming the scattering data to reconstruct the electron density.[12] The size and packing of the scattering objects are accurately and faithfully represented. As can be seen from the mathematical details below, the representation selected in not a unique solution.

This model process is based on work by Chan, who in 1965 proposed a scheme for generating a three-dimensional morphology of phase-separated materials by clipping a Gaussian random field ($\Psi(r)$) generated by supposing 10 000 isotropically propagating sinusoidal waves with random phases.[17] In this scheme the essential features of the morphology depends only on the spectral density function, $f(k)$, which is the inverse Fourier transform of the two-point correlation function, $g(r)$, of the Gaussian random field. The spectral density function gives the distribution of the magnitudes of the propagation wave vectors of the sinusoidal waves. Berk further developed the idea of Cahn mathematically for the purpose of analyzing scattering data.[18] Berk's contribution was to relate the two-point correlation function and the Debye correlation function ($\Gamma^{\alpha}(r)$) which determines the scattering intensity. Later, Chen et al. elaborated on this idea for more disordered morphologies, which accurately reproduce small-angle scattering data.[19] This technique has been used to look at other bicontinuous phase materials.[32]

The model is based on the fundamental assumption that the material is isotropic, indicating global isotopy, which does not rule out local anisotropy and that the material consists of only two phases. The absence of directional variation in the two-dimensional scattering of the solution-cast films was sufficient to support this assumption in this work. The only necessary input to the CRW analysis, other than the scattering data itself, is the porosity. Values found in the literature for Nafion[20,21] and the short side chain ionomer produced by Dow,[22] both similar polymers to the 3M ionomer, were averaged to attain the porosity used for generating the CRW morphology. Nafion porosity value varied from 0.28 to 0.4[21−23] while the Dow ionomer showed a slightly higher porosity, 0.45−0.45.[21] A porosity value of 0.35 (pore volume/total volume) was used for both dry and wet samples. The dry film most certainly has a lower porosity than that of the water-swollen films. However, a constant porosity was chosen to reduce the assumptions used and highlight the physical changes as determined by the changes in the SAXS.

In generating the morphology, the following steps are performed:

Calculate the Debye correlation function from the measured SAXS intensity, $\Gamma^{\alpha}(r)$:

$$\Gamma^{\alpha}(r) = \int_0^{\infty} \left(4\pi q^2 I(q) \frac{\sin(qr)}{qr}\right) \mathrm{d}q \qquad (8)$$

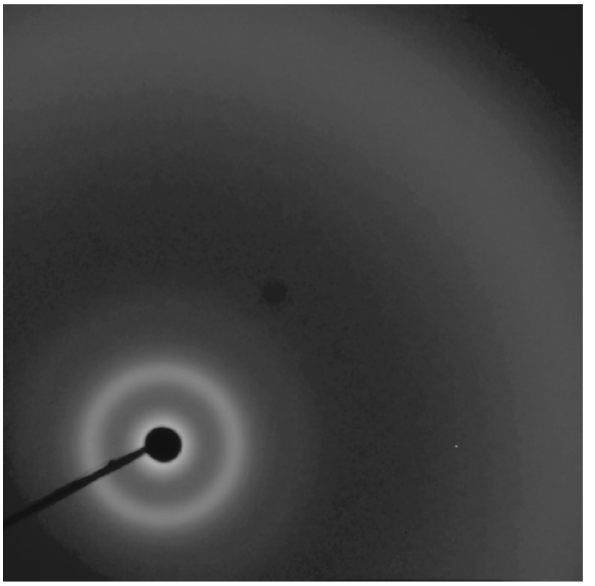

Figure 1. 2D scattering from one of the hydrated PFSA membranes, showing no anisotropy.

From this the two-point correlation function $g(r)$ is obtained:

$$\Gamma^{\alpha}(r) = \Gamma^{\alpha}(0) - \frac{1}{2\pi} \int_{g(r)}^{\infty} \left(\mathrm{e}^{-\alpha^2/(1+t)} \frac{1}{\sqrt{1-t^2}}\right) \mathrm{d}t \qquad (9)$$

$\Gamma^{\alpha}(0)$ is the "true volume fraction" (1-porosity). The porosity is a defined value. α, the clipping parameter, is related to the porosity and calculated via

$$\Gamma^{\alpha}(0) = \frac{1}{\sqrt{2\pi}} \int_{\alpha}^{\infty} (\mathrm{e}^{-x^2/2}) \, \mathrm{d}x \qquad (10)$$

A Gaussian random field is generated by summing 10 000 cosine waves with random phases where the magnitudes of the wave vectors are obtained from the spectral function $f(k)$. The spectral function is the inverse Fourier transform of $g(r)$:

$$f(k) = \int_0^{\infty} 4\pi r^2 g(r) \frac{\sin kr}{kr} \, \mathrm{d}r \qquad (11)$$

In calculating the morphology, a three-dimensional array is constructed using $f(k)$ and the Gaussian random field. If the value at a given point in the array is less than α, then the corresponding voxel is deemed solid. This has been implemented in the SAXSMorph program[24] and visualized using POV-Ray. 50 Å slices were taken from each CRW model and analyzed using ImageJ graphical analysis software. Only objects with a projected area greater than 100 Å^2 were considered.

4. Results and Discussion

4.1. Numerical Fitting. A typical SAXS image is shown in Figure 1. As can be seen from the figure and as expected, these solution-cast samples showed no directional anisotropies in the two-dimensional scattering pattern. The q range scanned, 0.01−0.2 Å^{-1}, allowed the resolution of both the so-called ionomer peak and the crystalline domains of the polymer. The SAXS patterns of both the "dry" as-cast films and water-boiled films are shown in Figure 2. Examining the scattering features from high to low q, for the boiled, water-swollen films, the three distinct regions are observed: (1) The

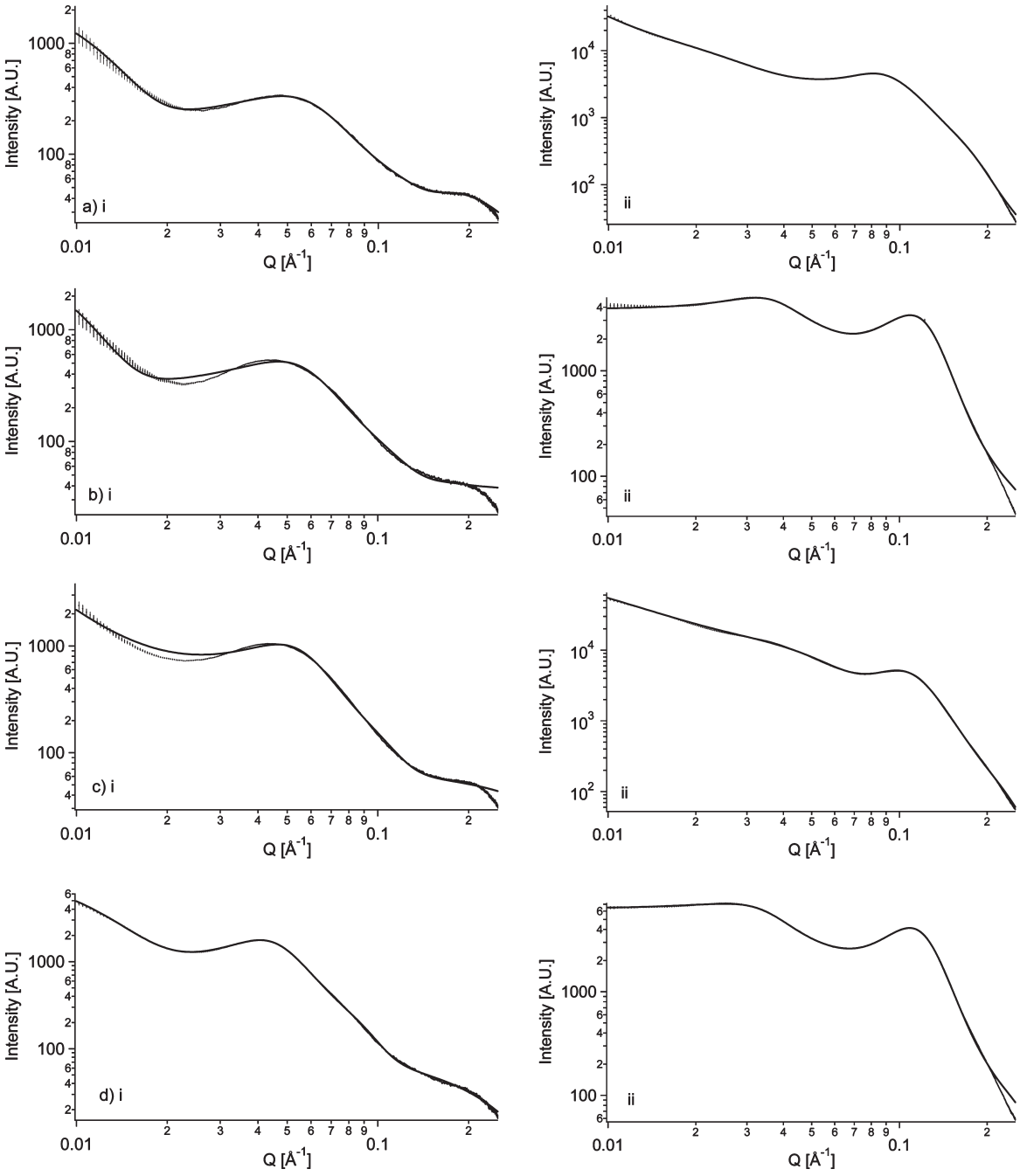

Figure 2. Experimental data and unified fits for (a) 733, (b) 825, (c) 900, and (d) 1082 both (i) as-cast and (ii) after boiling in DI water.

ionomer peak or agglomeration of the hydrophilic portions of the polymer chain occurs near 0.1 Å^{-1} in the hydrated membranes. This is due to an increase in both size and abundance of these domains as compared to the relatively broad peak near 0.21 Å^{-1} in the dry films. (2) The crystalline backbone or ordering of the PTFE-like crystallites can be seen in the q range between 0.02 and 0.06 Å^{-1}. These larger structures are packed close enough to interfere with each other, which is characterized by a broad peak in this range. (3) While not present in all films, some samples show increasing intensity up to the low-q detection limit. This can be seen q range below 0.02 Å^{-1}. The feature (if present) is attributed to large structures not able to be resolved in our angular range. Other researchers have attributed this to large chain-to-chain features such as a macromolecular lamellae.[25]

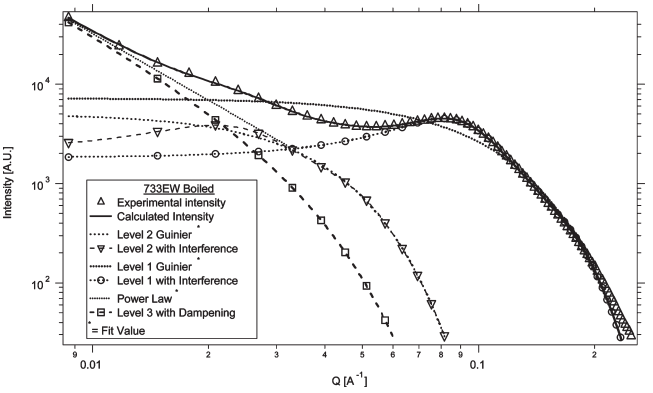

Figure 3. Components of numerical fitting for a 733 EW boiled film of the ionomer.

Table 1. Unified Fit Parameters for As-Cast "Dry" and Boiled, "Wet" Ionomer Films

	733 dry	733 wet	825 dry	825 wet	900 dry	900 wet	1082 dry	1082 wet
level 1 R_g [Å]	4.7 (3)	17.43(0.1)	6.63 (4)	16.16 (1)	6 (1)	16.09 (1)	12.1 (6)	16.45 (1)
level 1 G	48(1)	7205(3)	63(1)	5940(3)	70 (10)	7524 (10)	435 (48)	7651 (4)
level 1 η [Å]	30.7 (4)	62.0 (1)	29 (fixed)	48.3 (1)	30.6 (7)	51.1 (1)	17 (1)	48.3 (1)
level 1 pack	1.58 (5)	2.95 (1)	1.46 (3)	5.10 (1)	1.1 (2)	4.74 (1)	4.3 (5)	4.94 (1)
level 1 R_g CO [Å]	N /A	N /A	N /A	N /A	N /A	N /A	N /A	N /A
level 2 R_g [Å]	24.86 (7)	48.2 (6)	26.59 (3)	39.023 (2)	28.8 (1)	30.48 (1)	34.32 (2)	45.22 (2)
level 2 G	480.3 (7)	5045 (8)	764.4 (8)	5961 (4)	1655 (2)	148 (9)	2605 (2)	9111 (7)
level 2 η [Å]	97.9 (1)	235.9 (7)	102.8 (8)	151.8 (1)	103.9 (1)	139.1 (1)	124.95 (3)	172.9 (1)
level 2 pack	1.60 (1)	1.3 (2)	1.83 (1)	1.66 (1)	1.95 (1)	1.66 (1)	2.99 (1)	1.16 (1)
level 2 R_g CO [Å]	N/A	N/A	N/A	N/A	N/A	N/A	N/A	N/A
level 3 P	1.6 (4)	2.24 (2)	2.3 (8)	N/A	1.17 (1)	1.18 (1)	2.08 (2)	N/A
level 3 B	2 (1)	1.1 (1)	0.1 (5)	N/A	227 (9)	227 (9)	0.35 (3)	N/A
level 3 R_g Co [Å]	152	50	187	N/A	160.81	50	86	N/A

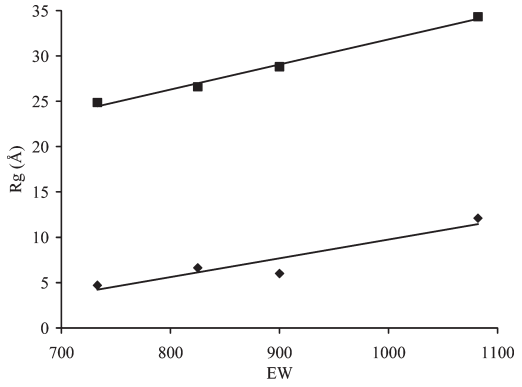

Figure 4. R_g for the hydrophobic crystalline (■) and the hydrophilic ionomer domains (◆) of the "dry" ionomer films.

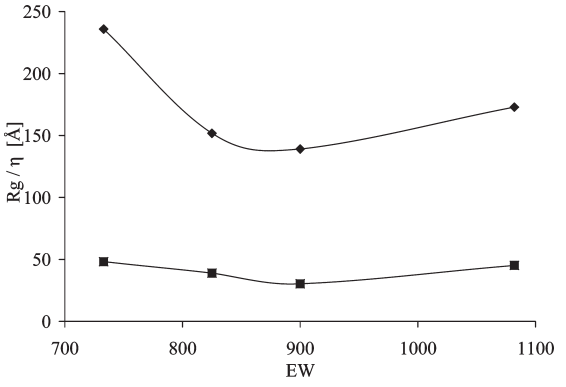

Figure 5. Radius of gyration (■) and center-to-center spacing (◆) of hydrophobic region of water-swollen films PFSA films of varying EW.

Numerical fitting was performed using the Irena macros for Igor Pro.[15] A typical deconvolution of all components to the numerical fitting is shown in Figure 3. The numerical fitting provided fits that were in excellent agreement with the data. This can be seen by the visual representation of the data and fits, in Figure 2, and is tabulated, along with fitting errors in Table 1. The radius of gyration, of the ionic domains, was found to be within the range of most previous studies of PFSA ionomers.[26−29] The increasing number of sulfonic acid sites per volume on a polymer chain does not appear to increase the size of the ionic domains. Rather, these domains maintain a constant R_g between 30.1 and 31.4 Å. The growth in the size and abundance of the ion-conducting channels is apparent from the raw data. The scattering data reflect this in the ionomer peak: increase in intensity and a shift to lower q, respectively.

It can be seen from the data in Table 1 that the scattering objects pack quite closely. The R_g of ionic domains of the fully hydrated membranes varies between 16.09 and 17.34 Å. If a spherical structure is assumed, this equates to diameters between 20.77 and 22.51 Å. The center-to-center distance is calculated to be between 48.35 and 62.01 Å. The resulting void space is between ionic clusters is between 5.9 and 17.0 Å. The 733 EW ionomer shows 6% larger ionic domain size and contributes significantly to the variance in the data. These values are in agreement with some of the more recent morphological models of ionic domains that have been presented for Nafion.[30] For the dry films there is a linear relationship between the R_g of both the hydrophobic crystalline and the hydrophilic ionomer domains, as shown in Figure 4. For the crystalline domains this is obviously not surprising, as at higher EW there will be more hydrophobic backbone in the material. It is curious that at least in the "dry" as cast film that this also forces the initial ionomer clusters to be larger.

Particularly within the range of equivalent weights between 825 and 1082, an abundance of sulfonic acid per PTFE repeat unit appears not to be the main driving force in the size of the ionic domains in the 3M ionomer. This suggests that an ionic domain size corresponding to an R_g near 16 Å is in a lower energy state than other sized formations. At equivalent weights below 825 the polymer may behave in a more gel-like fashion, particularly after boiling, and therefore account for the larger domain sizes.

Correlations between crystalline regions of the dry films show an increase in the packing variable (eq 5) from a value of 1.5 for the 733 EW ionomer to 2.0 for the 1082 EW ionomer, a 33% increase. This indicates the ratio of the volume of the crystallites volume to total volume increases with equivalent weight. This result is expected as higher EW films have a higher percentage of $(-C-F_2-)$ repeat units and therefore have more crystalline material present. As the membranes become hydrated the distance between crystalline structures increases from an average of 13.0 Å in the dry films to 17.4 Å in the fully hydrated samples. This is consistent with water swelling in the channels, which is also visible from the representation of the autocorrelation function.

Recent reviews of shorter side chain ionomers, in comparison to Nafion, have suggested that the metric of most importance for proton conduction in PFSA PEMs is to lower the EW as much as possible while maintaining good viscoelastic properties. This study of ionomers of compatible equivalent weights but with different length side chains concluded that the ionomer with the shorter side chain

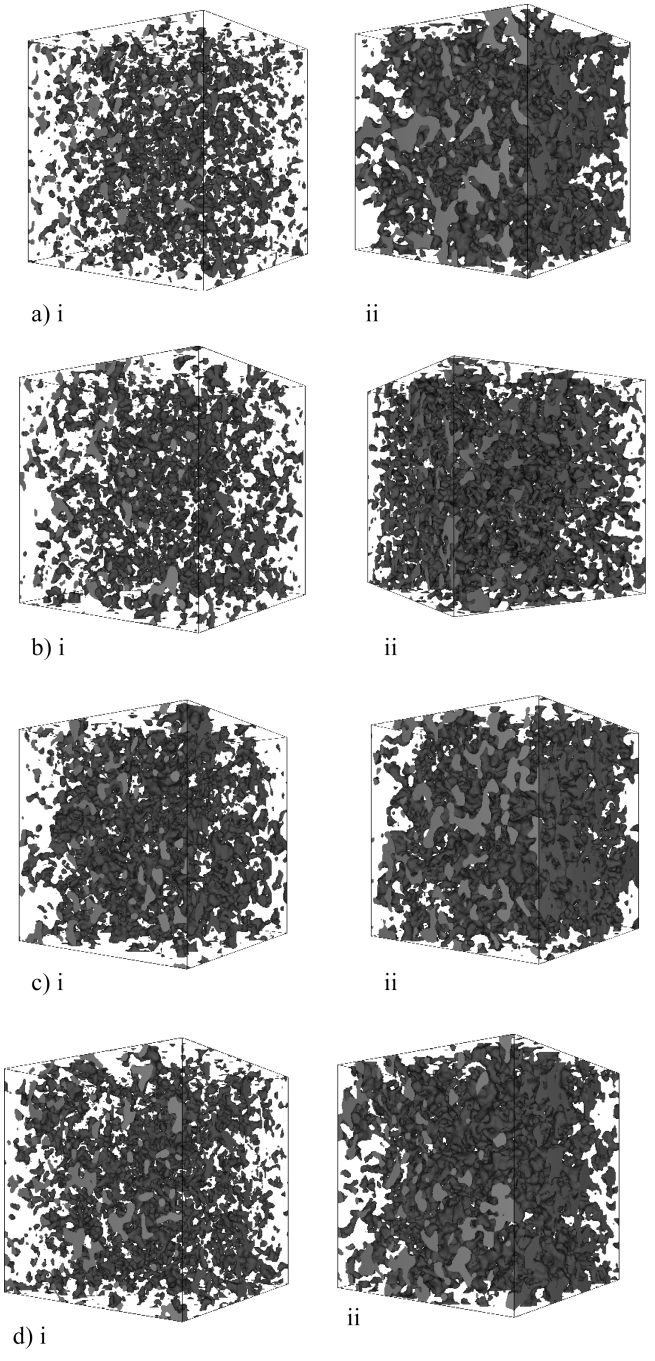

Figure 6. CRW representations showing the hydrophilic channels as solids for (a) 733, (b) 825, (c) 900, and (d) 1082 both (i) as-cast and (ii) after boiling in DI water. Cubes are 1000 Å per side.

showed better viscoelastic properties along with higher protonic conductivity over a wide range of temperatures[31] As can be seen in Figure 5, the 733 EW spacing of the crystallites, an indicator of in situ viscoelastic properties, increases sharply. This highlights the most desirable balance between low equivalent weights and mechanical properties as seen by crystallite spacing.

4.2. CRW Representations. The visualizations of the random waves that have been appropriately clipped by the spectral function $f(k)$ are shown in Figure 6. It is clear that while holding porosity constant the visual representation of the water channels grows in size and abundance in the postboiled state. The network shown does not show interconnectivity for the dry films as would be expected in PFSA type membranes. This is most likely due to our computational limitations that forced us to use a grid that may be too coarse. Therefore, it is the ensemble average that determines whether the CRW at a given point is deemed solid or part of a water channel. However, network connectivity can clearly be seen in the wet films. From the image analysis of the slices of the CRWs, the projected surface area of the water was measured. The average and standard deviations for each analysis are summarized in Table 2. The results of the CRW method give areas that are from 2 to 4 times larger than would be calculated from the data in Table 1, if we were to assume a spherical model ($R_g^2 = 3R^2/5$). This fact seems to strongly support the observed morphology in Figure 6 which shows features with an aspect ratio greater than 1, as the limit for an infinitely thin ribbon model would give $R_g^2 = L^2/12$. No anisotropy in the scattering is observed, indicating that these features have a random orientation.

Table 2. Image Analysis of the CRW Morpholgies for As-Cast "Dry" and Boiled, "Wet" Ionomer Films

	average size [Å^2]	std dev [Å^2]
733 EW dry	65.3	60.8
733 EW boiled	2176	3408
825 EW dry	727	771
825 EW boiled	3386	3506
900 EW dry	1260	1480
900 EW boiled	2094	3189
1082 EW dry	784	873
1082 EW boiled	2182	3553

The size of the proton conducting channels calculated via this method is between 20.0 and 26.4 Å. There are distinct similarities between the appearance of our model and results from recent dissipative particle dynamic (DPD) calculations.[9,10] The value of our measured domain size is ~50% less than the calculated value by DPD; however, the standard deviation in this measurement is large. The conclusion from the DPD study was that the average water channel size for the 3M ionomer is between 50 and 60 Å. However, our results align closely with other modeling techniques recently presented. The results are also consistent with the dimensions of the ionic domains in the so-called "parallel water channel" model[30] which was applied to 1100 EW Nafion. However, in contrast to those published results, our results do not indicate parallel features of any kind.

5. Conclusions

The problem of understanding the microstructure of the 3M ionomer PFSA films has been approached from two different yet complementary angles. The first, a numerical approach, utilizes a very simple model to determine the radius of gyration of different scattering features of the ionomer films. The interactions in this model are accounted for by treating the particles as spheres. Packing densities and spacing are calculated from the model. The second approach makes no assumptions about the material other than it is isotropic. Then, using only the scattering data and a porosity parameter, a random wave is clipped to produce a real-space image of the microstructure. The results of the two data analysis techniques can be correlated with each other if we assume that the particles actually are randomly orientated objects with an aspect ration greater than 1. In addition, the CRW model shows striking similarities to the structure proposed in recent DPD modeling studies[9,10] and is reasonable in the context of most previously proposed models.

In contrast to the simplest established model,[6] we chose to use a morphological model that does not assume regular shapes, while the correlations presented in this work are calculated for spheres, which were chosen simply out of mathematical simplicity, rather

than to support any conceptual model. So the calculated R_g can be applied to a variety of different geometric representations. The morphologies generated are representative morphologies; i.e., they have the same scattering behavior (give the same SAXS pattern) as the sample. The morphology generated is not a unique solution. As the sample scattering had no anisotropy either in space or shape, the morphology calculation is valid.

We have quantified some of the observations made by Kreuer et al.[31] that trade-offs between backbone rigidity and crystallinity and equivalent weight need to be made. It was clear that below 825 EW crystallites were more distantly spaced and may not provide the necessary mechanical support.

This has been the first time to our knowledge that the CRW technique has been applied to a PFSA type ionomer. The CRW technique has allowed for a visualization of the microstructure of a PFSA polymer in its hydrated form with minimal assumptions. Applications of this technique should be applied to the development new polymer systems for PEMFC development, particularly in the context of materials less reliant on water for ion transport.

Acknowledgment. ChemMatCARS Sector 15 is principally supported by the National Science Foundation/Department of Energy under Grant CHE-0535644. Use of the Advanced Photon Source was supported by the U.S. Department of Energy, Office of Science, Office of Basic Energy Sciences, under Contract DE-AC02-06CH11357. The work carried out here was directly supported by the U.S. Department of Energy, Cooperative Agreement DE-FC36-02AL67621. DOE support does not constitute an endorsement by DOE of the views expressed in this paper. A.M.H. thanks 3M for a nontenured faculty award.

References and Notes

(1) Turner, J. A. *Science* **1999**, *285*, 687−689.
(2) Hamrock, S. J.; Yandrasits, M. A. *Polym. Rev.* **2006**, *46*, 219–244.
(3) Emery, M.; Frey, M. H.; Guerra, M.; Haugen, G.; Hintzer, K.; Lochhaas, K. H.; Pham, P.; Pierpont, D.; Schaberg, M.; Thaler, A.; Yandrasits, M. A.; Hamrock, S. J. *Electrochem. Soc. Trans.* **2007**, *11*, 3–14.
(4) Arcella, V.; Troglia, C.; Ghielmi, A. *Ind. Eng. Chem. Res.* **2005**, *44*, 7646–7651.
(5) Mauritz, K. A.; Moore, R. B. *Chem. Rev.* **2004**, *104*, 4535–4586.
(6) Gierke, T. D.; Munn, G. E.; Wilson, F. C. *J. Polym. Sci.: Polym. Phys. Ed.* **1981**, *19*, 1687−1704.
(7) Kreuer, K. D.; Paddison, S. J.; Spohr, E.; Schuster, M. *Chem. Rev.* **2004**, *104*, 4637–4678.
(8) Gebel, G. *Polymer* **2000**, *41*, 5829–5838.
(9) Wu, D.-S.; Paddison, S. J.; Elliott, J. A. *Macromolecules* **2009**, *42*, 3358–3367.
(10) Wu, D.-S.; Paddison, S. J.; Elliott, J. A. *Energy Environ. Sci.* **2008**, *1*, 284–293.
(11) Yammamoto, S.; Hyodo, S.-A. *Polym. J.* **2003**, *35*, 519–527.
(12) Elliott, J. A.; Hanna, S. *J. Appl. Crystallogr.* **1999**, *32*, 1069–1083.
(13) Guinier, A.; Fournet, G. *Small-Angle Scattering of X-rays*; Wiley: New York, 1955.
(14) Beaucage, G.; Schaefer, D. W. *J. Non-Cryst. Solids* **1994**, *172*−*174*, 797–805.
(15) Beaucage, G. *J. Appl. Crystallogr.* **1995**, *28*, 717–728.
(16) Riello, P.; Benedetti, A. *J. Chem. Phys.* **1997**, *106*, 8660–8663.
(17) Cahn, J. *J. Chem. Phys.* **1965**, *42*, 93.
(18) Berk, N. F. *Phys. Rev. Lett.* **1987**, *58*, 2718.
(19) Chen, S.-H.; Chang, S.-L.; Strey, R. *J. Appl. Crystallogr.* **1991**, *24*, 721–731.
(20) Lehmani, A.; Turq, P.; Périé, M.; Périé, J.; Simonin, J.-P. *J. Electroanal. Chem.* **1997**, *428*, 81–89.
(21) Verbrugge, M. W.; Schneider, E. W.; Conell, R. S.; Hill, R. F. *J. Electrochem. Soc.* **1992**, *139*, 3421–3428.
(22) Verbrugge, M. W.; Hill, R. F. *J. Electrochem. Soc.* **1990**, *137*, 3770–3777.
(23) Divisek, J.; Eikerling, M.; Mazin, V.; Schmitz, H.; Stimming, U.; Volfkovich, Y. M. *J. Electrochem. Soc.* **1998**, *145*, 2677–2683.
(24) http://www.irl.cri.nz/SAXSfiles.aspx.
(25) Kim, M. H.; Glinka, C. J.; Grot, S. A.; Grot, W. G. *Macromolecules* **2006**, *39*, 4775–4787.
(26) Manley, D. S.; Williamson, D. L.; Noble, R. D.; Koval, C. A. *Chem. Mater.* **1996**, *8*, 2595−2600.
(27) Gebel, G.; Lambard, J. *Macromolecules* **1997**, *30*, 7914−7920.
(28) Haubold, H. G.; Vad, T.; Jungbluth, H.; Hiller, P. *Electrochim. Acta* **2001**, *46*, 1559−1563.
(29) Paddison, S. J.; Paul, R. *Phys. Chem. Chem. Phys.* **2002**, *4*, 1158–1163.
(30) Schmidt-Rohr, K.; Chen, Q. *Nat. Mater.* **2008**, *7*, 75–83.
(31) Kreuer, K.; Schuster, M.; Obliers, B.; Diat, O.; Traub, U.; Fuchs, A.; Klock, U.; Paddison, S.; Maier, J. *J. Power Sources* **2008**, *178*, 499–509.
(32) Hedstrom, J. A.; Toney, M. F.; Huang, E.; Kim, H.-C.; Volksen, W.; Magbitang, T.; Miller, R. D. *Langmuir* **2003**, *20*, 1535–1538.